X-Ray Fluorescence Analysis

Parth Bhargava · A0310667E

PC3193 Experimental Physics II

March 29, 2026

1 Abstract

X-ray fluorescence (XRF) spectroscopy was used for qualitative elemental identification of unknown samples and quantitative composition analysis of a brass alloy. In Part 1, calibrated spectra from a Fe+Zn reference target were used to assign characteristic line energies to six unknowns: brass (Cu, Zn, Pb), a magnetic sample (Sm, Co), old/new 50-cent coins (Cu, Ni), an old 1-dollar coin (Cu-rich, no resolved Ni line), and a new 1-dollar coin (Cu, Ni). Observed line energies agreed with tabulated values to within ± 0.08 keV in all cases, and K_β/K_α intensity ratios fell in the expected range of 1/5 –1/10, confirming consistent identification. In Part 2, Gaussian deconvolution resolved the Cu K_β / Zn K_α overlap near 8.7 keV in the brass spectrum. Using the manual's first-order mass-ratio relation and five repeated trials, the brass composition was estimated as Cu $(60.8 \pm 8.0)\%$, Zn $(36.6 \pm 7.7)\%$, Pb $(2.6 \pm 3.3)\%$, consistent with leaded brass. The dominant source of uncertainty was run-to-run scatter in the Pb reference spectrum (H_0 ranging from 453 to 868), reflecting the sensitivity of the weak Pb L_α line to sample positioning.

2 Introduction

X-ray fluorescence is a non-destructive elemental analysis technique based on inner-shell ionisation and radiative relaxation. When a primary X-ray photon ejects a core electron from an atom, the resulting vacancy is filled by an electron from a higher shell, and the energy difference is emitted as a characteristic X-ray photon. Because the relevant transitions involve tightly bound inner-shell electrons, characteristic line energies depend almost entirely on atomic number and are only weakly affected by chemical bonding. As a consequence, the spectrum of a multi-element sample is approximately the superposition of the spectra of its constituent elements, making XRF well suited for both qualitative identification and quantitative composition analysis.

This experiment has two objectives:

- **Qualitative analysis (Part 1)**: identify the elements present in brass, a magnetic sample, and old/new Singapore coins by matching observed peaks to tabulated characteristic line energies and verifying self-consistency through K_β/K_α intensity ratios.
- **Quantitative analysis (Part 2)**: estimate mass fractions in brass from fitted Gaussian peak heights relative to pure-element reference spectra, using repeated measurements to assess reproducibility.

3 Theory

3.1 Characteristic X-ray Emission

When an incident photon ejects a K-shell electron, the vacancy can be filled by an electron from the L-shell (K_α transition) or M-shell (K_β transition). For a given element, the K_β line lies at higher energy than K_α because the M-to-K energy gap exceeds the L-to-K gap, and its intensity is characteristically 1/5 to 1/10 that of K_α due to lower transition probability.

For heavy elements such as lead ($Z = 82$), the K-shell binding energy (88 keV) far exceeds the X-ray tube voltage used in this experiment (35 kV). K-shell ionisation is therefore energetically impossible, and only L-series transitions are observed: L_α ($M \to L$, 10.55 keV), L_β ($N \to L$, 12.61 keV), and L_γ (14.76 keV).

Moseley's law provides the approximate scaling of line energy with atomic number:

$$\sqrt{E} = a(Z - \sigma) \tag{1}$$

where a and σ are constants for a given series. This monotonic relationship means that elements of similar Z produce lines close in energy. In particular, Ni K_β (8.265 keV) and Cu K_α (8.044 keV) are separated by only 0.22 keV and are unresolvable by a semiconductor detector with typical resolution ΔE `approx` 0.2 keV at these energies.

3.2 Quantitative First-Order Model

Consider a homogeneous sample of element i irradiated by X-rays. The number of fluoresced atoms contributing to the measured peak height H_i is proportional to the number density of that element in the irradiated volume. If the sample has cross-sectional area S and effective irradiation depth d, the number of atoms of element i is:

$$n_i = \frac{\rho_i S d}{A_i} \tag{2}$$

where ρ_i is the bulk density and A_i the atomic mass. In a first-order approximation neglecting matrix effects (self-absorption, secondary fluorescence, and composition-dependent attenuation), the peak height is proportional to n_i:

$$H_i \ \texttt{prop}\ n_i \ \texttt{prop}\ \rho_i \tag{3}$$

For the same element measured as a pure reference, the peak height $H_{0,i}$ is proportional to its full bulk density. The ratio $H_i \ / \ H_{0,i}$ thus estimates the effective fraction of the irradiated volume occupied by element i. The mass fraction is then:

$$C_i = \frac{\rho_i H_i \ / \ H_{0,i}}{\sum_j \rho_j H_j \ / \ H_{0,j}} \tag{4}$$

This model assumes all elements are measured under identical geometry and that the detector response is uniform across the energy range of interest. In practice, matrix effects — self-absorption and composition-dependent attenuation — cause systematic deviations from this first-order relation.

3.3 Gaussian Deconvolution of Overlapping Peaks

In the brass spectrum, Cu K_β (`approx` 8.90 keV) partially overlaps Zn K_α (`approx` 8.64 keV). Reading peak heights directly would overestimate the Zn contribution. The CASSY software resolves this by fitting the 7.5–9.1 keV region with multiple Gaussians:

$$N(E) = \sum_k A_k e^{-(E-\mu_k)^2 \ / \ (2\sigma^2)} \tag{5}$$

where A_k is the amplitude, μ_k the centre (fixed to the known line energy), and σ is constrained to be equal for all components within a fit region. This separates the Cu K_α, Cu K_β, and Zn K_α amplitudes for use in Equation 4.

4 Methods

4.1 Instrument and Settings

The X-ray tube (Mo anode) was operated at 35 kV and 1 mA. Fluorescent X-rays were detected at 90° to the primary beam using a Si semiconductor detector coupled to a multi-channel analyser

(MCA) with 512 channels. Each spectrum was recorded for 300 s. The target angle was set to 45° to maximise the irradiated area (see Table 6 in Appendix).

4.2 Energy Calibration

Calibration was performed using the Fe+Zn reference target. The two strongest peaks — Fe K_α (6.403 keV) and Zn K_α (8.638 keV) — were assigned in the CASSY Lab software to establish the linear channel-to-energy conversion. This two-point calibration defines the energy axis for all subsequent spectra.

4.3 Part 1: Qualitative Analysis Procedure

After calibration, spectra were recorded for six samples by placing each in the sample holder and acquiring for 300 s:

1. Brass (Target 3)
2. Magnetic sample (Target 4)
3. Old 50-cent coin
4. New 50-cent coin
5. Old 1-dollar coin
6. New 1-dollar coin

Element identification used two criteria: (i) the observed peak energy was matched to tabulated values (Bearden 1967), and (ii) the presence of a consistent line family was verified — for K-series elements, both K_α and K_β should appear with the latter at `approx` 1/5–1/10 the intensity.

4.4 Part 2: Quantitative Brass Analysis Procedure

For the quantitative analysis of brass, the CASSY software's Gaussian fitting tool was used to decompose the overlapping Cu–Zn region. The fit region (channels `approx` 195–240) was modelled with three Gaussians (Cu K_α, Zn K_α, Cu K_β) sharing a common width, with centres fixed at the known line energies. A separate single-Gaussian fit was used for Pb L_α (channels `approx` 260–285).

This procedure was repeated five times (trials 2–6) for the brass sample and four times each for the pure Cu, Zn, and Pb reference targets, repositioning the sample between trials to capture the effect of geometric variability. All fit parameters were saved as CASSY `.labx` project files, from which the Gaussian amplitudes (A_k) were extracted programmatically.

5 Results

5.1 Part 1: Calibration and Qualitative Identification

The calibration spectrum (Figure 1) shows the four expected peaks from the Fe+Zn target. Fe K_α and Zn K_α were used to define the energy scale; the positions of Fe K_β and Zn K_β provide an independent check of calibration linearity.

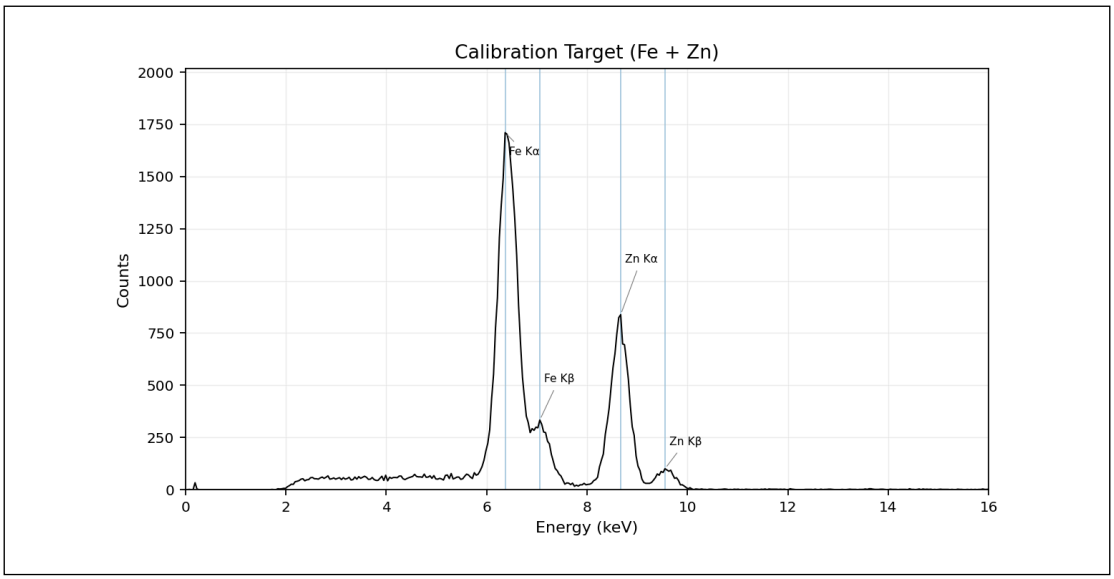

Figure 1: Calibration spectrum (Fe + Zn target, 300 s). The Fe K_α (6.40 keV) and Zn K_α (8.67 keV) peaks define the linear energy calibration. Fe K_β and Zn K_β appear at approximately 1/5 and 1/8 the respective K_α intensities. The broad feature below approx 5 keV is the Bremsstrahlung continuum from the Mo tube.

The calibration data also allow a check of the K_β/K_α intensity ratio. For Fe, this ratio is $333/1710 = 0.195$ approx 1/5.1; for Zn it is $100/838 = 0.119$ approx 1/8.4. Both fall within the expected 1/5–1/10 range, confirming that the identification method is self-consistent.

Figure 2 shows the brass spectrum. Cu K_α and Zn K_α dominate, with partial overlap of Cu K_β and Zn K_α near 8.7 keV. A weak Pb L_α line is visible at 10.55 keV. The presence of Pb L_β (12.7 keV) and a marginal Pb L_γ (14.7 keV) confirms the Pb assignment through the full L-series pattern.

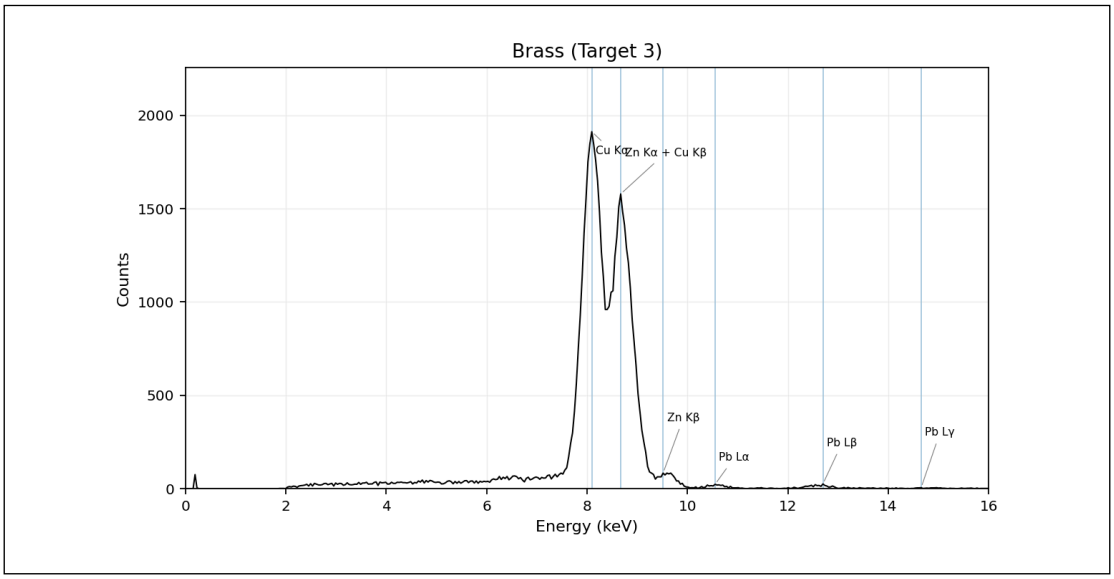

Figure 2: Brass (Target 3) spectrum, 300 s. Cu K_α (8.09 keV) and Zn K_α + Cu K_β (merged near 8.7 keV) dominate. Pb is confirmed by the complete L-series: L_α (10.55 keV), L_β (12.7 keV), and L_γ (14.7 keV, barely above noise).

The magnetic sample (Figure 3) contains Co and Sm, consistent with a SmCo-type rare-earth permanent magnet. The Co K_β/K_α ratio of $98/654 = 0.150$ (approx 1/6.7) is within the expected range.

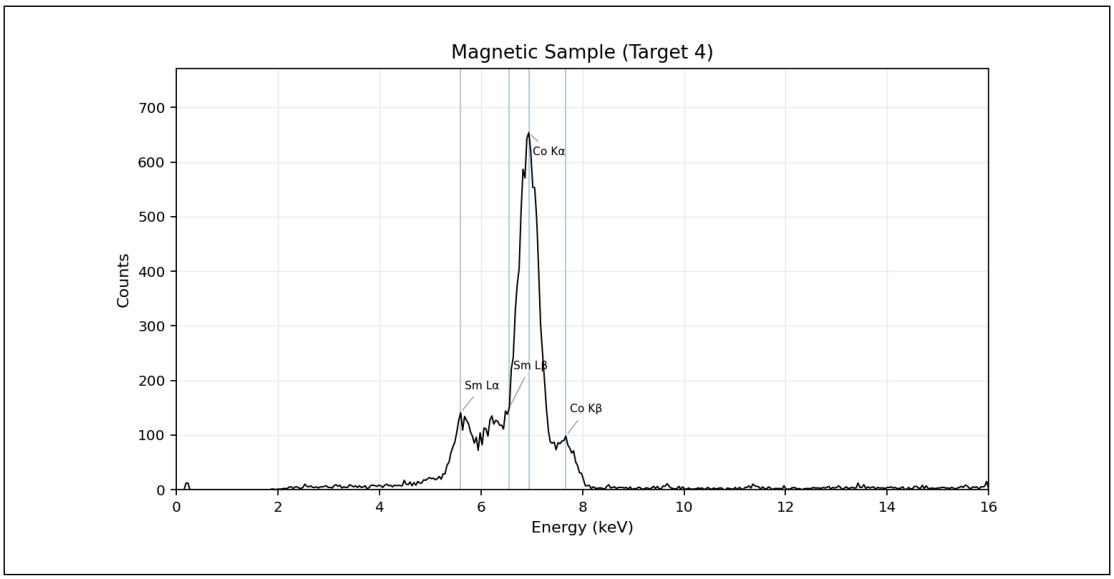

Figure 3: Magnetic sample (Target 4) spectrum. The dominant feature is Co K_α (6.94 keV), with Co K_β at 7.67 keV. Sm is identified from its L_α (5.60 keV) and L_β (6.48 keV) lines.

The four coin spectra are shown in Figure 4 through Figure 7. The old and new 50-cent coins (Figure 4 and Figure 5) are both Cu-Ni alloys, with Ni K_α and Cu K_α clearly resolved. In these spectra, the Ni K_β (8.265 keV) and Cu K_α (8.044 keV) lines are separated by only 0.22 keV, which is below the detector resolution; they merge into a single unresolved peak labelled "Cu K_α + Ni K_β" in the plots.

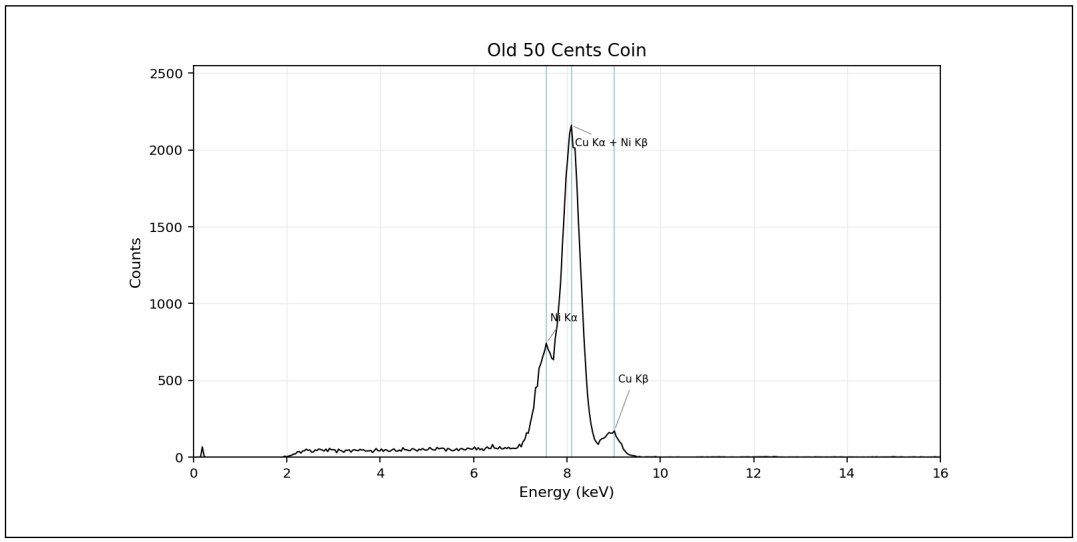

Figure 4: Old 50-cent coin spectrum. The Ni K_α shoulder at 7.56 keV is clearly resolved from the dominant Cu K_α + Ni K_β blend at 8.09 keV, confirming a Cu-Ni alloy.

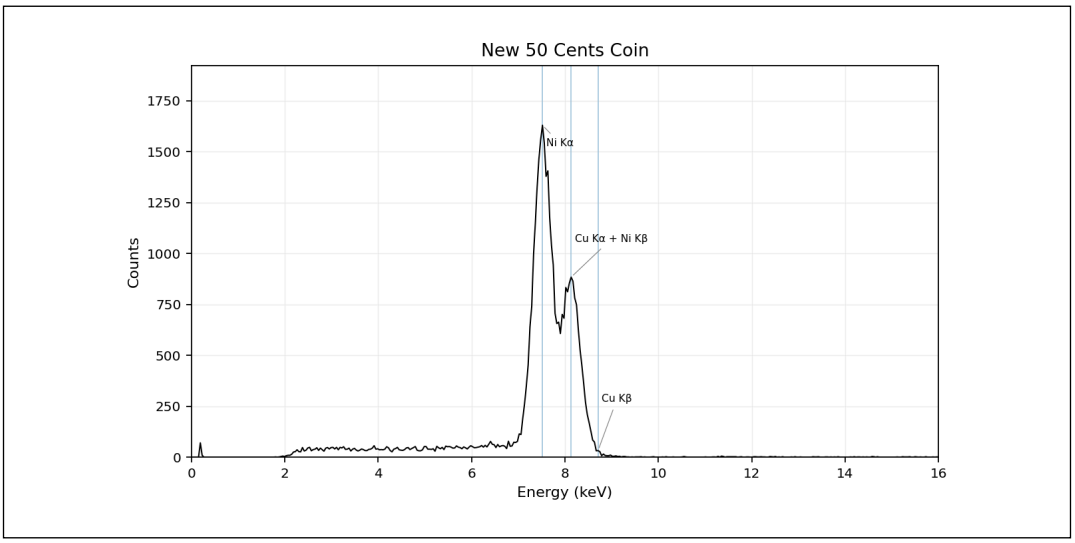

Figure 5: New 50-cent coin spectrum. Similar Cu-Ni alloy signature as the old coin, with comparable relative peak intensities.

The old 1-dollar coin (Figure 6) shows only Cu lines with no Ni feature. This is consistent with an aluminium bronze composition (Cu-Al-Zn) used in older Singapore dollar coins, where Al and Zn are either below the detection threshold or outside the calibrated energy window. The new 1-dollar coin (Figure 7) shows both Ni and Cu, indicating a change to a cupronickel-based alloy in newer mintages.

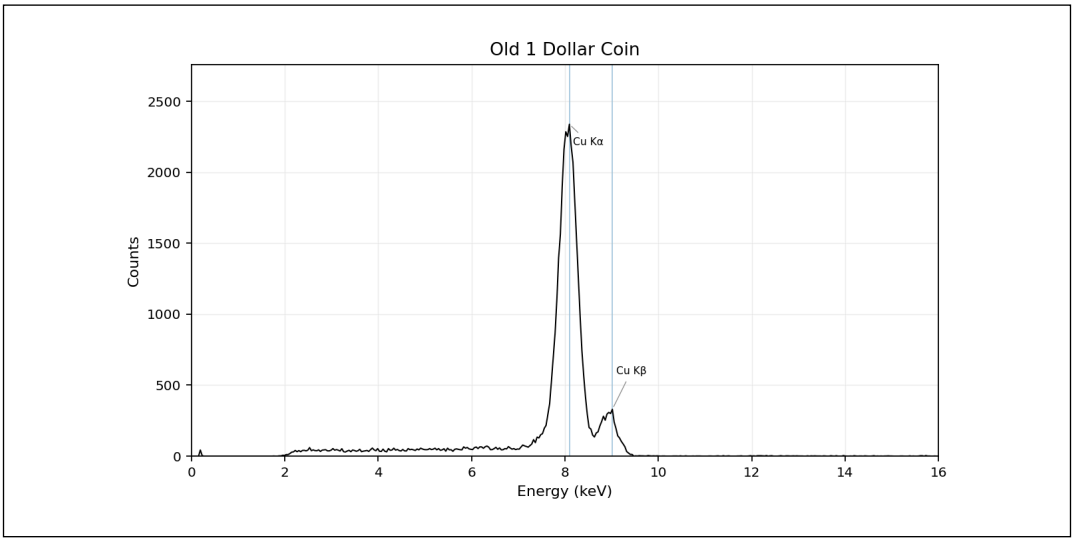

Figure 6: Old 1-dollar coin spectrum. Only Cu K_α (8.09 keV) and Cu K_β (9.01 keV) are present. The Cu K_β/K_α ratio of $330/2338 = 0.141$ (`approx` $1/7.1$) is consistent with a pure Cu-based alloy.

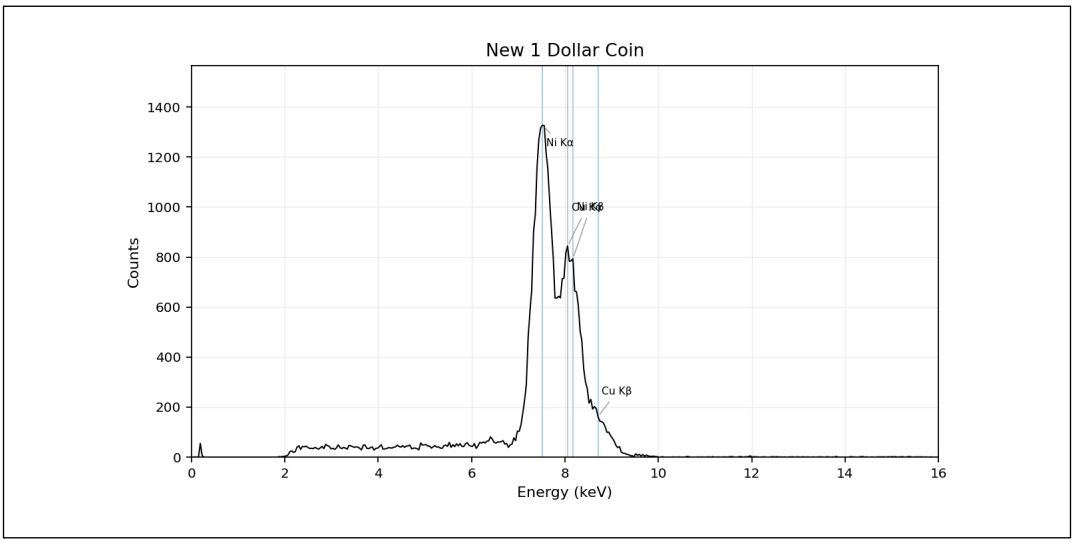

Figure 7: New 1-dollar coin spectrum. Both Ni K_α (7.52 keV) and the Cu K_α / Ni K_β blend (8.1 keV) are visible, confirming a Cu-Ni alloy composition.

Table 1 compares observed peak energies to literature values across the calibration and brass spectra. Deviations are within ± 0.08 keV for isolated lines. The two-point linear calibration introduces small nonlinear residuals at energies far from the calibration points, as seen in the +0.08 keV offset of Pb L_β at 12.7 keV.

Line	**Literature (keV)**	**Observed (keV)**	**Δ (keV)**
Fe K_α	6.403	6.367	−0.036
Fe K_β	7.057	7.058	+0.001
Zn K_α	8.638	8.669	+0.031
Zn K_β	9.572	9.551	−0.021
Cu K_α (brass)	8.044	8.094	+0.050
Pb L_α (brass)	10.551	10.549	−0.002
Pb L_β (brass)	12.614	12.697	+0.083

Table 1: Observed vs. literature (Bearden 1967) line energies. The two calibration anchors (Fe K_α, Zn K_α) are assigned exactly; deviations in other lines reflect calibration residuals.

Sample	**Main observed lines (keV)**	**No. elements**	**Identified composition**
Brass (Target 3)	8.09, 8.67, 10.55, 12.70	3	Cu + Zn + Pb
Magnetic sample (Target 4)	5.60, 6.48, 6.94, 7.67	2	Sm + Co
Old 50 cents	7.56, 8.09, 9.01	2	Ni + Cu
New 50 cents	7.52, 8.13, 8.75	2	Ni + Cu
Old 1 dollar	8.09, 9.01	1	Cu-rich alloy (no resolved Ni)
New 1 dollar	7.52, 8.06, 8.75	2	Ni + Cu

Table 2: Qualitative identification summary. Energies are observed peak centres; assignment uses line-energy matching and line-family consistency.

5.2 Part 2: Quantitative Brass Composition

The Gaussian deconvolution of the brass spectrum is shown in Figure 8. The fit separates the Cu K_α, Zn K_α, and Cu K_β contributions in the overlap region, with the sum of the individual Gaussians (dashed) closely tracking the measured spectrum (solid).

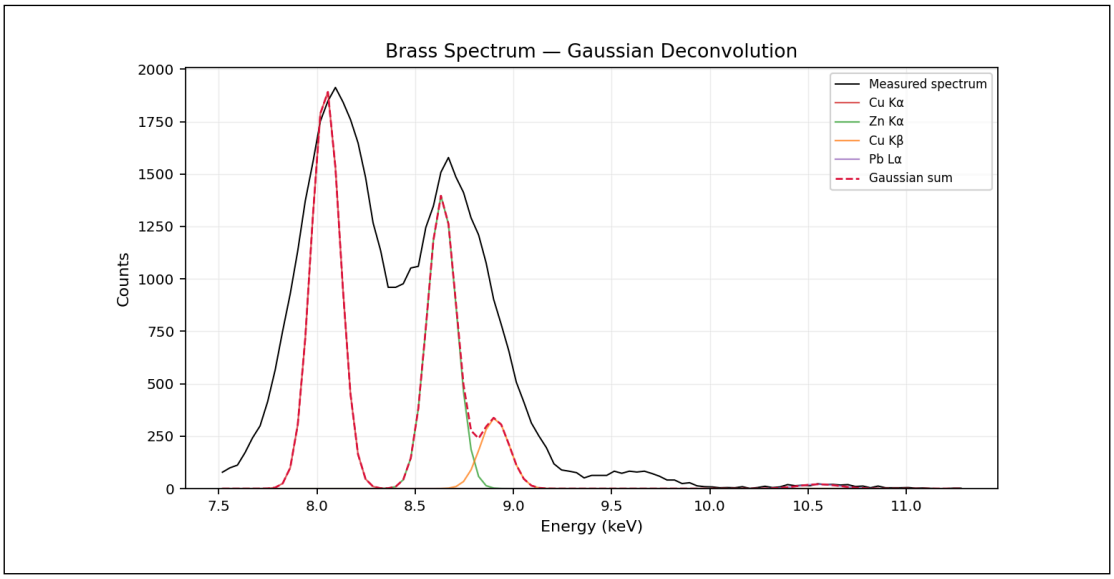

Figure 8: Gaussian deconvolution of the brass spectrum in the 7.5–11.3 keV region. The Cu K_α (red), Zn K_α (green), Cu K_β (orange), and Pb L_α (purple) Gaussians are shown individually, with their sum (dashed crimson) overlaid on the measured spectrum (black). Gaussian amplitudes have been scaled to match the Part 1 qualitative spectrum.

Table 3 lists the extracted Gaussian amplitudes from each trial, showing the spread that propagates into the final composition uncertainty.

Trial	$\boldsymbol{H_{\mathrm{Cu}}}$	$\boldsymbol{H_{\mathrm{Zn}}}$	$\boldsymbol{H_{\mathrm{Pb}}}$
Brass trial 2	2742.6	2005.3	29.5
Brass trial 3	1979.8	1474.7	23.3
Brass trial 4	1797.2	1253.8	21.9
Brass try 5	2520.2	1906.9	23.5
Brass try 6	1744.1	1243.3	19.4
Mean ± s.d.	**2156.8 ± 448.9**	**1576.8 ± 360.0**	**23.5 ± 3.7**

Table 3: Gaussian fit amplitudes (H_i) for brass across five trials. The `approx` 1.6 × variation in Cu and Zn amplitudes reflects repositioning between trials.

Element	**Trial 1**	**Trial 2**	**Trial 3**	**Trial 4**
Cu (H_0)	1976.5	1894.9	1760.7	1688.3
Zn (H_0)	1714.2	1606.9	1860.6	1891.4
Pb (H_0)	867.5	590.1	481.2	452.8

Table 4: Reference spectrum amplitudes ($H_{0,i}$) for pure elements. Pb shows the widest spread (452–868), reflecting geometric sensitivity of the weak L_α line.

Using the mean values from Table 3 and Table 4 in Equation 4 yields the mass fractions in Table 5.

Element	ρ (g/cm^3)	Line	H / H_0	$\rho \cdot H$ / H_0	C_i (%)
Cu	8.96	K_α	1.179	10.56	60.8
Zn	7.14	K_α	0.892	6.37	36.6
Pb	11.34	L_α	0.039	0.45	2.6

Table 5: Mass-ratio calculation for brass using Equation 4 and mean fitted heights from Table 3 and Table 4.

Monte Carlo propagation (50 000 draws from the measured run-to-run distributions) gave:

- Cu: $(60.3 \pm 8.0)\%$
- Zn: $(36.6 \pm 7.7)\%$
- Pb: $(3.1 \pm 3.3)\%$

The uncertainties are dominated by the scatter in reference amplitudes (H_0), especially for Pb where H_0 ranges nearly $2\times$ across four trials.

6 Discussion

6.1 Calibration Quality and Systematic Energy Offsets

The two-point calibration using Fe K_α and Zn K_α assumes a linear channel-to-energy conversion. Table 1 shows that this assumption holds well for energies near the calibration range (6–10 keV), with deviations of at most ± 0.05 keV. At higher energies (Pb L_β at 12.7 keV), the deviation grows to $+0.08$ keV, consistent with a slight nonlinearity in the detector response at the edge of the calibrated range. This systematic offset does not affect qualitative identification, as the shifts remain small compared to inter-element line spacings (> 0.5 keV between neighbouring elements).

6.2 Spectral Background: Bremsstrahlung Continuum

All spectra exhibit a broad, featureless hump below approx 5 keV. This is the Bremsstrahlung (continuous X-ray) spectrum from the Mo-anode tube, whose maximum energy is set by the 35 kV accelerating voltage. The continuum is not relevant for peak identification but contributes to background counts under low-energy lines. In this experiment, all characteristic peaks of interest lie above 5.6 keV where the continuum has largely decayed, so background subtraction has minimal impact on the results.

6.3 Unresolved Overlaps: Ni K_β and Cu K_α

In the Cu-Ni coin spectra (Figure 4, Figure 5, Figure 7), the Ni K_β line (8.265 keV) and Cu K_α line (8.044 keV) are separated by only 0.22 keV. With the Si detector's energy resolution of approximately 0.2 keV FWHM in this range, these lines cannot be individually resolved. The merged peak in the coin spectra is therefore a blend of both transitions. Fortunately, elemental identification is unambiguous because each element is independently confirmed by its resolved line: Ni by K_α at 7.48 keV and Cu by K_β at 8.9 keV. A quantitative Cu-to-Ni ratio for the coins would require Gaussian deconvolution analogous to what was done for brass.

6.4 Counting Statistics and Measurement Sensitivity

Poisson statistics govern the uncertainty in photon counting: $\sigma_N = \sqrt{N}$. For strong peaks such as Cu K_α in the old 1-dollar spectrum (N approx 2340), the statistical uncertainty is σ/N approx 2.1 %, which is negligible compared to systematic effects. In contrast, the Pb L_α peak in brass has only approx 23 counts above background, giving σ/N approx 21%. The net-peak uncertainty, including background subtraction, is:

$$\sigma_{\text{net}}^2 = \sigma_{\text{peak}}^2 + \sigma_{\text{bkg}}^2 \tag{6}$$

For weak lines like Pb L_α, background counts under the peak are comparable to the signal, further degrading the signal-to-noise ratio.

6.5 Effect of Measurement Time

Signal counts scale linearly with acquisition time t, while SNR improves as $\sqrt{t}$. At the 300 s used in this experiment:

- Halving the time to 150 s would reduce Cu K_α counts from approx 1900 to approx 950, increasing its statistical noise from 2.3% to 3.2%. Weak lines like Pb L_α (approx 12 counts) would become unreliable.
- Doubling to 600 s would improve SNR by $\sqrt{2}$, giving more stable Gaussian fits — particularly beneficial for Pb, where the approx 21% statistical noise on 23 counts would reduce to approx 15 % on approx 46 counts.

6.6 Matrix Effects and Model Limitations

Equation 4 neglects several physical effects:

- **Self-absorption**: Cu K_α photons (8.04 keV) can be absorbed by Cu atoms in the sample before reaching the detector, systematically lowering H_{Cu} relative to a pure reference.
- **Secondary fluorescence**: in a multi-element sample, characteristic photons from one element can excite fluorescence in another if the photon energy exceeds the absorber's edge energy. In brass, Cu K_α (8.04 keV) is below the Zn K-edge (9.66 keV), so Cu does not enhance Zn. However, in alloys containing Ni (K-edge 8.33 keV), Zn K_α (8.64 keV) could excite secondary Ni fluorescence.
- **Detector efficiency**: the Si detector efficiency varies with photon energy. This variation partially cancels in the ratio $H_i/H_{0,i}$ because alloy and reference spectra are measured with the same detector.

These effects are modest for first-order composition estimates but can introduce systematic biases of several percent. The reported Cu/Zn/Pb values should therefore be interpreted as approximate.

6.7 Coin Composition and Magnetism

The key spectral differences between coins are:

- **Old/new 50-cent**: both show Cu + Ni, consistent with cupronickel alloy (typically 75% Cu, 25% Ni).
- **Old 1-dollar**: Cu lines only, with no resolved Ni peak. This is consistent with the aluminium bronze composition (Cu-Al-Zn) used in pre-2013 Singapore 1-dollar coins. Al (K_α at 1.49 keV) falls below the detector's practical sensitivity range.
- **New 1-dollar**: Cu + Ni lines, indicating a switch to a nickel-plated steel or cupronickel composition.

Regarding magnetism: XRF probes only the near-surface layer of a sample (penetration depth approx 10–100 μm for metals in this energy range). If a coin has a ferromagnetic steel core beneath a Cu-Ni plating, the Fe signal from the core would be attenuated or completely absorbed by the plating. Therefore, the absence of Fe lines in the XRF spectrum does not exclude a steel core. Magnetic behaviour in the new coins likely arises from such a steel substrate, but this cannot be confirmed by XRF surface analysis alone.

6.8 Quantitative Result Quality

The central composition estimate (Cu approx 61%, Zn approx 37%, Pb approx 2–3%) is physically plausible for leaded brass (standard C36000 free-cutting brass is 61.5% Cu, 35.5% Zn, 3% Pb). The main limitation is run-to-run scatter: H_{Cu} varies by a factor of approx 1.6 × across five trials (1744

to 2743), and H_0 for Pb spans nearly $2\times$ (453 to 868). This scatter exceeds what Poisson statistics alone would predict (σ/N approx 2–5% for peaks of this magnitude) and is attributed to variations in sample positioning, which changes the solid angle subtended by the detector and the effective irradiated volume.

The fact that the Cu:Zn ratio remains relatively stable across trials ($H_{\mathrm{Cu}}/H_{\mathrm{Zn}} = 1.30$–$1.40$) despite the absolute amplitude swings confirms that geometric effects largely cancel in relative measurements, supporting the ratio-based approach of Equation 4.

7 Conclusion

The XRF experiment successfully achieved both objectives. Qualitative analysis identified all constituent elements across six unknowns using characteristic line energies and K_β/K_α ratio consistency checks, with observed energies agreeing with tabulated values to within ± 0.08 keV. Quantitative analysis of brass, after Gaussian deconvolution of the Cu K_β / Zn K_α overlap, yielded a composition of Cu approx 61%, Zn approx 37%, Pb approx 2–3%, consistent with standard leaded brass. The dominant source of quantitative uncertainty was run-to-run geometric variability rather than counting statistics, demonstrating both the power and the practical limitations of uncorrected first-order peak-height methods in XRF composition analysis.

8 References

1. X-Ray Fluorescence Analysis (PC3193 lab manual), provided.
2. J.A. Bearden, "X-ray wavelengths," **Rev. Mod. Phys. 39**, 78 (1967).
3. C. Kittel, **Introduction to Solid State Physics**, 8th ed., Wiley (2005), chapters on X-rays and scattering.

9 Appendix

9.1 Instrument Settings

Parameter	**Value**
Tube anode	Mo
Tube voltage	35 kV
Tube current	1 mA
Measurement channels	512
Counting time	300 s
Detector	Si semiconductor
Detector angle	90°
Target angle	45°
Calibration target	Fe + Zn

Table 6: Operating settings used for XRF measurements.

10 Declaration on the Use of Generative AI

I declare that I **HAVE** used generative AI tools to produce this assignment.

I acknowledge that generative AI was used in the following manner:

AI Tool Used	**My Prompt and AI Output**	**How the Output Was Used**
Cursor / Claude Code	Prompt: "Process XRF CSV/LABX files, extract Gaussian fit parameters, and generate publication-quality plots and summary tables." Output: Python script and processed numerical summaries.	Used for data extraction/plotting automation. Final interpretation and report writing were verified and edited by me.
Cursor / Claude Code	Prompt: "Help structure the Typst report and format equations, figures, and tables for XRF analysis." Output: Typst layout guidance and draft text structure.	Used as drafting assistance. Physical interpretation, critical discussion, and final conclusions were written and checked by me.

Table 7: AI Tool Usage Declaration